ResearchGate

See discussions, stats, and author profiles for this publication at: https://www.researchgate.net/publication/216685459

Ferromagnetic Ordering, Anisotropy, and Spin Reorientation for the Cyano-Bridged Bimetallic Compound Mn 2 (H 2 O) 5 Mo(CN) 7 ·4H 2 O (α Phase)

ARTICLE *in* JOURNAL OF THE AMERICAN CHEMICAL SOCIETY · DECEMBER 1998

Impact Factor: 12.11 · DOI: 10.1021/ja9739953

CITATIONS
115

READS
30

6 AUTHORS, INCLUDING:

Joulia Larionova
Université de Montpellier
139 PUBLICATIONS **2,742** CITATIONS
SEE PROFILE

Joaquin Sanchiz
Universidad de La Laguna
86 PUBLICATIONS **2,685** CITATIONS
SEE PROFILE

Available from: Joaquin Sanchiz
Retrieved on: 25 January 2016

Ferromagnetic Ordering, Anisotropy, and Spin Reorientation for the Cyano-Bridged Bimetallic Compound $Mn_2(H_2O)_5Mo(CN)_7 \cdot 4H_2O$ (α Phase)

Joulia Larionova,[†] Rodolphe Clérac,[†,‡] Joaquin Sanchiz,[†] Olivier Kahn,*[,†] Stéphane Golhen,[§] and Lahcène Ouahab[§]

Contribution from the Laboratoire des Sciences Moléculaires, Institut de Chimie de la Matière Condensée de Bordeaux, UPR CNRS No. 9048, 33608 Pessac, France, Centre de Recherche Paul Pascal, UPR CNRS No. 8641, 33600 Pessac, France, and Laboratoire de Chimie du Solide et Inorganique Moléculaire, UMR CNRS No. 6511, Université de Rennes 1, 35042 Rennes, France

Received November 24, 1997. Revised Manuscript Received October 8, 1998

Abstract: The title compound has been synthesized by slow diffusion of aqueous solutions containing $K_4[Mo(CN)_7] \cdot 2H_2O$ and $[Mn(H_2O)_6](NO_3)_2$, respectively. The compound crystallizes in the monoclinic system, space group $P2_1/c$. The Mo site is surrounded by seven −C−N−Mn linkages in a distorted pentagonal bipyramid fashion. There are two distorted octahedral Mn sites, one with four and the other with three Mn−N−C−Mo linkages. The structure is three-dimensional and of low symmetry. It consists of ladders made of edge-sharing lozenge motifs $(MoCNMnNC)_2$ running along the *a* direction. These ladders are linked further along the *b* and *c* directions. Both temperature dependences of the magnetic susceptibility and field dependences of the magnetization have been investigated along the three crystallographic directions, *a*, *b*, and *c**. The angular dependence of the magnetization in the *ab* plane as a function of the external field has also been measured. These single crystal magnetic measurements have revealed that the compound orders ferromagnetically at $T_c = 51$ K, without hysteresis effect. Two additional magnetic phenomena have been detected. In zero field, another transition has been observed at 43 K, which disappears when applying a field higher than 100 Oe along the *a* direction. For a critical value of the field, H_c, applied along the *a* direction, a field-induced spin reorientation has been observed. The *b* direction is the easy magnetization axis in low field; both the *a* and *b* directions are easy magnetization axes as the external field overcomes the critical value. From the magnetic data, a magnetic phase diagram has been established. Finally, it has been found that when the compound is partially dehydrated, the long-range ferromagnetic ordering was shifted up to 65 K. This partially dehydrated material presents a magnetic hysteresis loop with a coercive field of 0.85 kOe at 5 K. The origins of the magnetic anisotropy along with the mechanism of the ferromagnetic interaction between low-spin Mo^{3+} and high-spin Mn^{2+} ions through the cyano bridge have been discussed.

Introduction

One of the very first synthetic coordination compounds ever reported, in 1710, is the Prussian blue (Berliner blau) of formula $Fe^{III}_4[Fe^{II}(CN)_6]_3 \cdot 15H_2O$ exhibiting a long-range ferromagnetic ordering at $T_c = 5.6$ K.[1−4] Prussian blue belongs to a vast family of Prussian blue-like phases with the general formula $A_k[B(CN)_6]_l \cdot nH_2O$, where A is high spin and B is low spin. The basic structure is faced-centered cubic with A−N−C−B linear linkages along three perpendicular directions.[5] Alkali-metal cations such as Cs^+ may occupy A_4 or B_4 tetrahedral sites. For $k > l$, some $B(CN)_6$ groups are missing, which creates a local breaking of the three-dimensional periodicity. These vacant sites are usually occupied by water molecules coordinated to the adjacent A atom.

In Prussian blue itself only the Fe^{3+} ions carry a local spin, and the interaction occurs between next-nearest neighbors. Much higher ordering temperatures have been reported when both A and B are magnetic centers. The compounds may then be three-dimensional ferri- or ferromagnets, depending on the nature of the A−B interaction through the cyano bridge. Owing to the high symmetry of the metal sites and of the symmetry as a whole, the symmetry rules between magnetic orbitals apply in a particularly heuristic fashion.[6]

The first magnetic studies concerning Prussian blue-like phases were reported by Bozorth and co-workers.[2] At the beginning of the eighties Klenze and co-workers[7] and then Babel and co-workers[8−11] characterized several phases with magnetic

[†] UPR CNRS No. 9048.
[‡] UPR CNRS No. 8641.
[§] UMR CNRS No. 6511.

(1) Anonymous. *Misc. Berolinensia Incrementum Scientiarum (Berlin)* **1710**, *1*, 377.
(2) Bozorth, R. M.; Williams, H. J.; Walsh, D. E. *Phys. Rev.* **1956**, *103*, 572.
(3) Holden, A. N.; Matthias, B. T.; Anderson, P. W.; Lewis, H. W. *Phys. Rev.* **1956**, *102*, 1463.
(4) Herren, F.; Fischer, P.; Ludi, A.; Hälg, W. *Inorg. Chem.* **1980**, *19*, 956.
(5) Ludi, A.; Güdel, H. U. *Struct. Bonding (Berlin)* **1973**, *14*, 1.
(6) Kahn, O. *Adv. Inorg. Chem.* **1995**, *43*, 179.
(7) Klenze, R.; Kanellakopoulos, B.; Trageser, G.; Eysel, H. *J. Chem. Phys.* **1980**, *72*, 5819.
(8) Griebler, W. D.; Babel, D. Z. *Z. Naturforsch. B* **1982**, *37*, 832.
(9) Babel, D. *Comments Inorg. Chem.* ***1986,*** *5*, 285.
(10) Babel, D.; Kurtz, W. In *Solid State Chemistry 1982*; Metselaar, R., Heijligers, H. J. M., Schoonman, J., Eds.; Elsevier: Amsterdam, 1983.
(11) Kurtz, W.; Babel, D. *Solid State Commun.* **1983**, *48*, 277.

10.1021/ja9739953 CCC: $15.00 © 1998 American Chemical Society
Published on Web 12/02/1998

ordering temperatures up to 90 K. More recently, two research groups led by Verdaguer[12−16] and Girolami,[17−19] respectively, initiated a thorough and systematic investigation of these Prussian blue-like phases and obtained compounds showing much higher critical temperatures. One of these phases reported by Verdaguer and co-workers, of formula $V^{II}_{0.42}V^{III}_{0.58}[Cr^{III}(CN)_6]_{0.86} \cdot 2.8H_2O$, is a ferrimagnet with a critical temperature of 310 K.[16] It should be noticed that this phase is nonstoichiometric and amorphous. In other respects, Hashimoto recently showed that some of these Prussian blue phases exhibited extremely interesting photomagnetic properties, due to light-induced electron transfers.[20]

One of the very appealing aspects of the studies dealing with Prussian blue-like phases resides in the fact that the magnetic characteristics of these compounds (nature of the interaction, saturation magnetization) are nicely in line with the theoretical models developed in molecular magnetism, even if those phases cannot be considered as being strictly molecular.[21] These very interesting materials, however, have some drawbacks. First, the basic structure of the Prussian blue-like phases is cubic, so that no magnetic anisotropy can be expected. Second, nobody so far succeeded to grow single crystals suitable for detailed physical measurements. In fact, it is now well established that these phases are often structurally disordered, with a certain degree of exchange between A and B sites. This situation led us to look for novel bimetallic extended lattices with cyano bridges whose symmetry would be much lower than that of Prussian blue phases. Another of our requirements was to obtain reasonably large single crystals allowing thorough single-crystal magnetic investigations. Furthermore, we recently initiated a project dealing with the use of 4d and 5d transition ions in molecular magnetism.[22] The conjunction of these two projects, 4d and 5d metal ions along with anisotropic cyano-bridged lattices, led us to utilize $[Mo(CN)_7]^{4-}$ as a precursor for obtaining new magnetic materials. This paper is devoted to the compound of formula $Mn_2(H_2O)_5Mo(CN)_7 \cdot 4H_2O$ (α phase). It is organized as follows: First the synthesis and the very anisotropic crystal structure are described. The heart of the paper deals with the single-crystal magnetic properties. These magnetic data will allow us to establish the peculiar magnetic phase diagram of the compound. The modification of the magnetic properties upon partial dehydration is then presented. Finally, the origin of the magnetic anisotropy is discussed along with the possible mechanisms of the interaction between low-spin Mo^{3+} and high-spin Mn^{2+} ions. A preliminary report of this work has already been published.[23]

Experimental Section

Synthesis. $K_4[Mo(CN)_7] \cdot 2H_2O$ was prepared as already described.[24,25] Well-shaped and rather large ($4 \times 0.5 \times 0.2$ mm^3) single crystals of the title compound were obtained by slow diffusion in a H-shaped tube under nitrogen of two deoxygenated 10^{-4} M aqueous solutions containing $K_4[Mo(CN)_7] \cdot 2H_2O$ and $[Mn(H_2O)_6](NO_3)_2$, respectively.[23] Actually, two kinds of crystals were obtained, denoted the α and β phase, respectively. The crystals of the α phase to which this paper is devoted have the shape of plates. The *a*, *b*, and *c* crystallographic axes correspond to the long, intermediate, and small edges, respectively (see Figure 6). The chemical formula of the β phase, $Mn_2(H_2O)_5Mo(CN)_7 \cdot 4.75H_2O$, is very close to that of the α phase. The local environments of the metal sites are also similar to what is described below. The three-dimensional organization, however, is significantly different, as well as the magnetic properties. A subsequent paper will be devoted to this β phase.

Crystallographic Data Collection and Structure Determination. Data were collected at room temperature on an Enraf-Nonius CAD4 diffractometer with use of Mo Kα radiation. After a semiempirical ψ-scan[26] absorption correction, the data reduction was performed using MOLEN[27] while structure solution and refinement were carried out using the programs SHELXS-86 and SHELXL-93.[28] Crystal data: $C_7H_{18}N_7O_9Mn_2Mo$, M = 558.10, monoclinic, space group $P2_1/c$, a = 7.951(5) Å, b = 16.819(3) Å, c = 15.189(6) Å, β = 104.29(2)°, V = 1969(2) Å^3, Z = 4, d_{calc} = 1.856 g·cm^{-3}, 3292 reflections observed [$I \geq 2\sigma(I)$], 287 variables, R = 0.0351, wR_2 = 0.0692, GOF = 1.090.

Magnetic Measurements. These were carried out with a Quantum Design MPMS-5S SQUID magnetometer working down to 2 K and up to 50 kOe. This apparatus was equipped with an horizontal goniometer. The compound is air sensitive, and all the magnetic investigations were carried out with either single crystals embedded in an oil envelop or polycrystalline samples placed in a quartz tube sealed under vacuum.

Description of the Structure

The structure contains a unique Mo site along with two manganese sites, denoted as Mn1 and Mn2, as shown in Figure 1. The molybdenum atom is surrounded by seven −C−N−Mn linkages, four of them involving a Mn1 site and three of them a Mn2 site. The geometry may be described as a slightly distorted pentagonal bipyramid, with Mo−C2−N2 and Mo−C7−N7 along the axial direction. The molybdenum coordination sphere is very close to that found in $NaK_3[Mo(CN)_7]$.[29] The C2−Mo−C7 angle is equal to 166.1(2)°. The C−Mo−C bond angles within the equatorial plane involving adjacent Mo−C bonds range from 72.3(2) to 75.8(2)°. The Mo−C bond lengths range from 2.127(4) to 2.174(4) Å. The Mo−C−N bond angles, as expected, are all close to 180°; they range from 175.8(4) to 178.7(4)°. On the other hand, some of the Mn−N−C bond angles deviate dramatically from 180°. They range from 139.1(3) to 174.3(3)°.

Both Mn1 and Mn2 sites are in distorted octahedral surroundings. Mn1 is surrounded by four −N−C−Mo linkages and two water molecules in *cis* configuration. The Mn1−N bond

(12) Gadet, V.; Bujoli-Doeuff, M.; Force, L.; Verdaguer, M.; Malkhi, K. E.; Deroy, A.; Besse, J. P.; Chappert, C.; Veillet, P.; Renard, J. P.; Beauvillain, P. In *Magnetic Molecular Materials*; Gatteschi, D., Kahn, O., Miller, J. S., Palacio, F., Eds.; NATO ASI Series E; Plenum: New York, 1991; Vol. 198.
(13) Gadet, V.; Mallah, T.; Castro, I.; Verdaguer, M. *J. Am. Chem. Soc.* **1992**, *114*, 9213.
(14) Mallah, T.; Thiébaut, S.; Verdaguer, M.; Veillet, P. *Science* **1993**, *262*, 1554.
(15) Mallah, T.; Ferlay, S.; Auberger, C.; Helary, C.; L′Hermite, F.; Ouahès, R.; Vassermann, J.; Verdaguer, M.; Veillet, P. *Mol. Cryst. Liq. Cryst.* **1994**, *273*, 141.
(16) Ferlay, S.; Mallah, T.; Ouahès, R.; Veillet, P.; Verdaguer, M. *Nature* **1995**, *378*, 701.
(17) Entley, W. R.; Treadway, C. R.; Girolami, G. S. *Mol. Cryst. Liq. Cryst.* **1994**, *273*, 153.
(18) Entley, W. R.; Girolami, G. S. *Science* **1995**, *268*, 397.
(19) Entley, W. R.; Girolami, G. S. *Inorg. Chem.* **1994**, *33*, 5165.
(20) Sato, O.; Iyoda, T.; Fujishima, A.; Hashimoto, K. *Science* **1996**, *272*, 704.
(21) Kahn, O. *Nature* **1995**, *378*, 667.
(22) Larionova, J.; Mombelli, B.; Sanchiz, J. Kahn, O. *Inorg. Chem.* **1998**, *37*, 679.
(23) Larionova, J.; Sanchiz, J.; Golhen, S.; Ouahab, L.; Kahn, O. *J. Chem. Soc., Chem. Commun.* **1998**, 953.
(24) Young, R. C. *J. Am. Chem. Soc.* **1932**, *54*, 1402.
(25) Rossman, G. R.; Tsay, F. D.; Gray, H. B. *Inorg. Chem.* **1973**, *12*, 824.
(26) North, A. C. T.; Philips, D. C.; Mathews, F. S. *Acta Crystallogr., Sect. A* **1968**, *A24*, 351
(27) *MOLEN (Molecular Structure Enraf-Nonius)*; Enraf-Nonius: Delft, The Netherlands, 1990.
(28) (a) Sheldrick, G. M. *SHELXS-86: Program for the Solution of Crystal* Structure, University of Göttingen: Göttingen, Germany, 1986. (b) Sheldrick, G. M. *SHELXL-93: Program for the Refinement of Crystal Structure*; University of Göttingen: Göttingen, Germany, 1993.
(29) Hursthouse, M. B.; Maijk, K. M. A.; Soares, A. M.; Gibson, J. F.; Griffith, W. P. *Inorg. Chim. Acta* **1980**, *45*, L81.

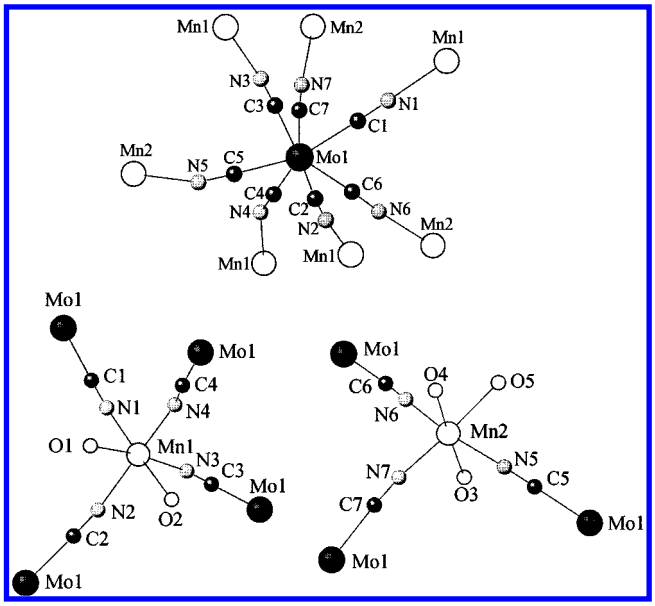

Figure 1. Local structure of the molybdenum and magnanese sites.

lengths range from 2.181(4) to 2.242(3) Å, and the Mn1−O bond lengths are equal to 2.181(4) and 2.308(4) Å, respectively. The bond angles around Mn1 do not deviate much from 90 and 180°. Mn2 is surrounded by three −N−C−Mo linkages and three water molecules in a pseudo C_{2v} symmetry. The Mn2−N bond lengths range from 2.183(4) to 2.232(4) Å, and the Mn2−O bond lengths, from 2.195(4) to 2.268(3) Å. Again, the bond angles are close to the ideal 90 and 180° values.

The three-dimensional organization may be described as follows: let us first consider the centrosymmetrical lozenge motifs $(MoC1N1Mn1N2C2)_2$ and $(MoC3N3Mn1N1C1)_2$, the former being more regular than the latter. These motifs alternate and share the MoC1N1Mn1 edge to form sorts of accordions or bent ladders running along the *a* direction, as shown in Figure 2. Each accordion is linked to four other accordions of the same kind along the [011] and [01$\bar{1}$] directions through Mo−C4−N4−Mn1 linkages (see Figure 4). Finally, the Mn2 site is not directly involved in the accordions but located between two adjacent accordions. It is linked to a Mo site of one of these accordions through the N5−C5 bridge and to two Mo sites of the other accordion through the N6−C6 and N7−C7 bridges, as shown in Figure 3. The structure as a whole viewed along the *a* direction is represented in Figure 4.

At the end of this section we point out the strong anisotropy of this structure. The *a* direction corresponds to the axis of the accordions. The *b* direction corresponds to infinite bimetallic linkages of the type Mo−C2−N2−Mn1−N4−C4− or Mo−C3−N3−Mn1−C4−N4−, with a zigzag shape. The *c* direction is more complex. It corresponds to the infinite linkages shown as in which the three metal sites are involved.

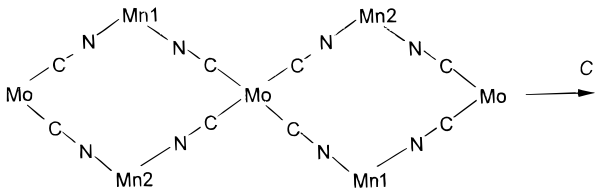

Magnetic Properties

In this section, we present some selected magnetic data which will allow us to characterize the magnetic phase diagram of the compound. All the magnetic measurements were carried out

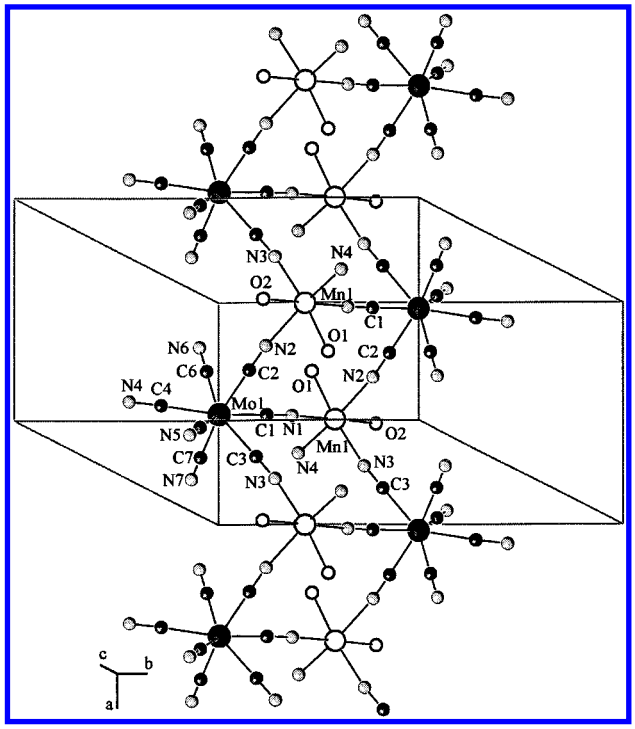

Figure 2. Structure of an accordion formed by alternation of two edge-sharing lozenge motifs along the *a* direction.

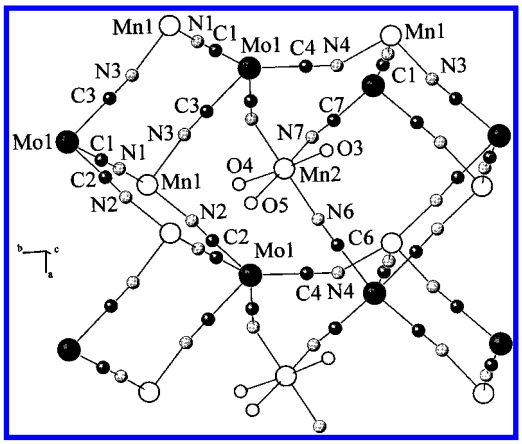

Figure 3. View showing how the Mn2 site is linked to two Mo sites of an accordion and one Mo site of an adjacent accordion.

on single crystals with the external field applied along the *a*, *b*, and *c** directions, except a preliminary $\chi_M T$ versus T curve carried out on a polycrystalline sample; χ_M is the magnetic susceptibility per $MoMn_2$ unit, and T the temperature.

Temperature Dependences of the Magnetic Susceptibility and Magnetization. The temperature dependence of $\chi_M T$, using a magnetic field of 6 kOe, is shown in Figure 5. At room temperature $\chi_M T$ is equal to 9.1 emu K mol^{-1}, which corresponds to what is expected for one low-spin Mo^{3+} and two high-spin Mn^{2+} uncorrelated ions with local spins $S_{Mo} = {}^1/_2$ and $S_{Mn} = {}^5/_2$. As T is lowered to ca. 50 K, $\chi_M T$ increases more and more rapidly and then reaches a maximum around 40 K. Such a curve reveals dominant ferromagnetic interactions, the maximum of $\chi_M T$ being due to saturation effects. The magnetic susceptibility data down to 51 K can be fitted with the Curie−Weiss law $\chi_M = C/(T - \Theta)$, with $C = 7.58$ emu K mol^{-1} and $\Theta = 51$ K (see the χ_M^{-1} versus T plot in the insert of Figure 5).

The temperature dependences of the magnetization, *M*, along the three crystallographic directions under a very weak external field, 5 Oe, are represented in Figure 6. The three curves exhibit

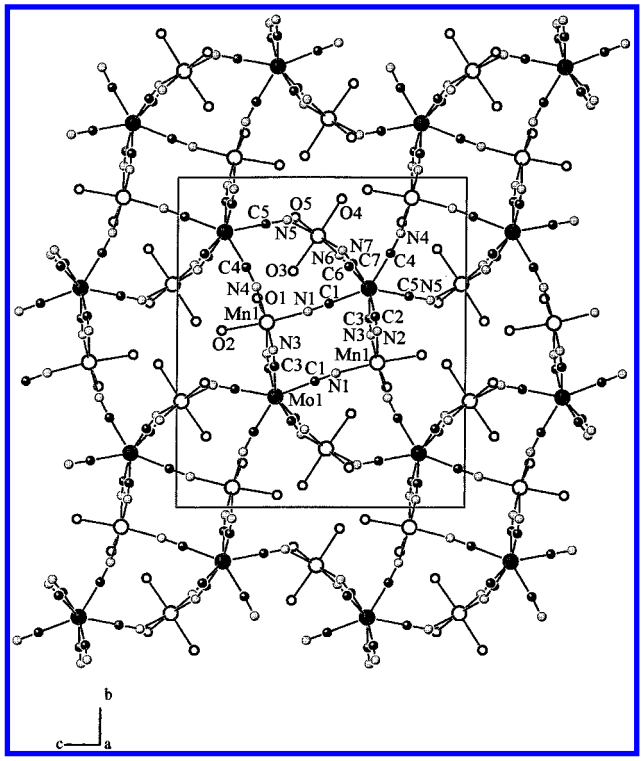

Figure 4. Structure of the compound viewed along the *a* direction.

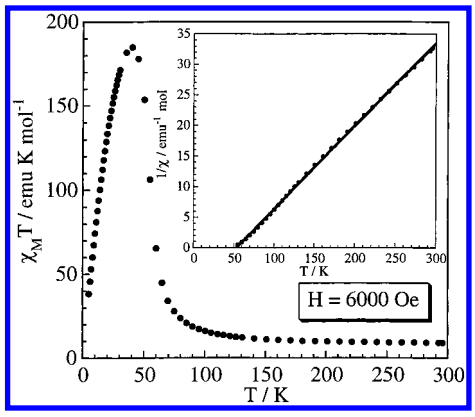

Figure 5. Temperature dependence of $\chi_M T$ for a polycrystalline sample. In the insert is shown the temperature dependence of $1/\chi_M$.

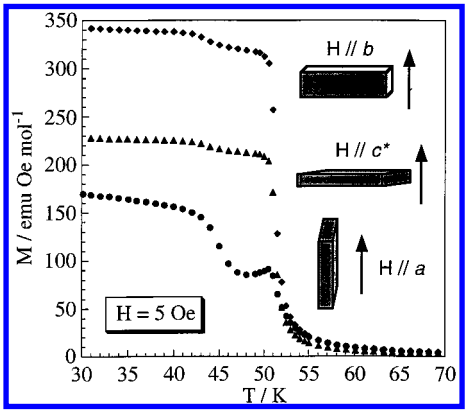

Figure 6. Temperature dependences of the magnetization along the *a*, *b*, and *c** directions, using an external field of 5 Oe.

a break below ca. 55 K with an inflection point at $T_c = 51$ K, characteristic of a long-range ordering, along with an anomaly at $T_c' = 43$ K. This anomaly is much more pronounced along the *a* direction than along the other two directions. In other respects, the magnetization induced by a field of 5 Oe is more important along the *b* than along the *a* and *c** directions. This *b* direction is the easy magnetization direction in zero or low field.

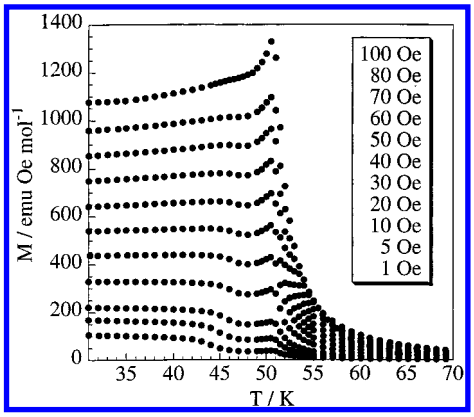

Figure 7. Temperature dependences of the magnetization along the *a* direction, using different values of the external field.

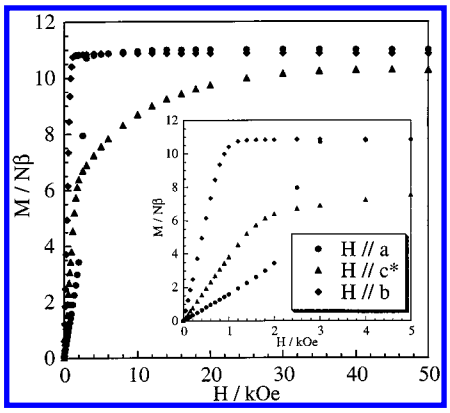

Figure 8. Field dependences of the magnetization at 5 K along the *a*, *b*, and *c** directions.

To obtain more insights on the magnetic anomaly detected at 43 K, visible essentially along the *a* direction, the magnetization along this direction was measured with an external field varying from 1 up to 100 Oe. The results are displayed in Figure 7. T_c' is shifted toward higher temperatures as the magnetic field increases and, eventually, for a field of ca. 100 Oe, merges with the transition at 51 K. For each field the transition temperature, T_c', was determined as the inflection point of the $M = f(T)$ curve. The $H = f(T_c')$ plot is used to define the border between domains II and III in the magnetic phase diagram of Figure 11.

Field Dependences of the Magnetization

Figure 8 represents the field dependences of the magnetization at 5 K along the *a*, *b*, and *c** directions. Let us note first that the curves are strictly identical when increasing and decreasing the field. In the magnetically ordered phase the compound exhibits no coercivity. Along the easy magnetization direction, *b*, the saturation is reached with ca. 1 kOe. The saturation magnetization is found equal to 11 $N\beta$. This value corresponds exactly to what is expected for the $S_{Mo} = {}^1/_2$ and $S_{Mn} = {}^5/_2$ local spins aligned along this direction. Along the *c** direction, the magnetization increases progressively when applying the field, and even at 50 kOe the saturation is not totally reached. Along the *a* direction, the *M* versus *H* curve is more complicated and reveals a peculiar behavior. *M* first increases smoothly as *H* increases, then very rapidly as *H* increases further, with an inflection point around 2.1 kOe, and eventually reaches the saturation value of 11 $N\beta$. This behavior is typical of a field-

induced spin reorientation phenomenon.[30−38] We can also notice a crossover of the curves along *a* and *c** for a field of 2.5 kOe. The hard axis is along *a* in low field and along *c** in high field. The critical field for which the spin reorientation is observed along the *a* direction depends on temperature. This is why the $M = f(H)$ curve along this direction was measured every 5 K in the ferromagnetic phase, and both H_c and H_{sat} were determined at each temperature, H_{sat} being the field for which the saturation is reached.[40] H_c was determined as the field correponding to the maximum of the derivative $\delta M/\delta H$. The $H_c = f(T)$ and $H_{sat} = f(T)$ curves are used to define the borders between domains I and IV and II and IV, respectively, in the magnetic phase diagram of Figure 11. H_c increases as T is lowered, reaches 2.2 kOe at 30 K, and seems to decrease very slightly as T is lowered further.

It must be specified that the $M = f(H)$ curves of Figure 8 are not corrected of the demagnetizing field. This correction is probably negligibly small along the *a* direction correponding to the long edge of the single crystal but may be more important along the other two directions. An attempt to take into account the demagnetizing field, assuming that the crystal had the shape of a long rod,[41] was carried out. It suggests that the slope of the $M = f(H)$ curve along the *c** direction in low field (up to ca. 2 kOe) is larger than shown in Figure 8. In low field the two magnetization curves, along *b* and *c**, might be closer to each other than shown in Figure 8.

Angular Dependence of the Magnetization in the *ab* Plane as a Function of the External Field. It was first checked that the magnetic axes were aligned with the crystallographic directions *a*, *b*, and *c**. To characterize the spin reorientation phenomenon in a thorough fashion, the angular dependence of the magnetization in the *ab* plane was investigated for several values of the external field between 1 and 3 kOe. The experiment was carried out at 10 K. The results are depicted in Figure 9. Under 1 kOe, the magnetization is maximum along the *b* direction ($\Theta = 0°$) and minimum along the *a* direction ($\Theta = 90°$); *b* is the easy magnetization axis. Under 2 kOe the minima are observed on either side of the *a* direction, and the magnetization along *a* ($\Theta = 90$) corresponds to a secondary maximum. The magnetization along *a* increases as the external field increases further, and under a field of 3 kOe, the magnetization along *a* is as high as or even slightly higher than along *b*. Both *a* and *b* become easy magnetization axes. It can be also noticed that the magnetic anisotropy in the *ab* plane decreases as the external field increases. This effect appears clearly in Figure 9 where the vertical coordinate is the magnetization *M*. It would appear even more spectacularly if the vertical coordinate was the susceptibility *M*/*H*.

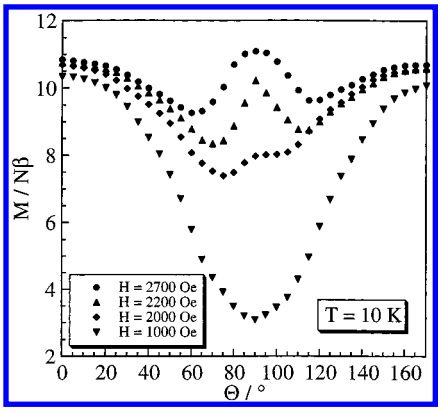

Figure 9. Angular dependence of the magnetization in the *ab* plane for different values of the external magnetic field.

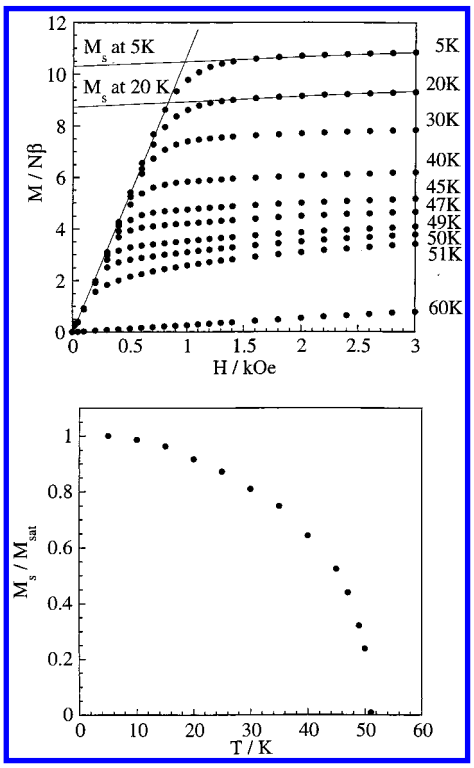

Figure 10. Top: Field dependences of the magnetization along the *b* direction at different temperatures. Bottom: Temperature dependence of the spontaneous (zero field) magnetization (see text).

Determination of the Spontaneous Magnetization. Applying an external field *H* on the sample results in an internal field H_i related to *H* through

$$H_i = H - NM \qquad (1)$$

where *N* is the demagnetizing factor depending on the shape of the sample. For instance, for a spherical crystal *N* is equal to $4\pi/3$, and for a long needle-shaped crystal *N* is negligibly small.[39] Equation 1 is valid in very low field. When the demagnetizing field compensates the external field, deriving (1) results in

$$M/H = 1/N \qquad (2)$$

It follows that *N* can be determined from the slope of the $M = f(H)$ curve at the origin, as shown in Figure 10 (top). At higher fields the demagnetizing field does not compensate the external field, and H_i is not zero anymore. The spontaneous magnetiza-

(30) Stryjewski, E.; Giordano, N. *Adv. Phys.* **1977**, *26*, 487.
(31) Givord, D.; Li, H. S.; Perrier de la Bathie, R. *Solid State Commun.* **1984**, *51*, 857.
(32) Hirosawa, S.; Matsuura, Y.; Yamamoto, H.; Fujimura, S.; Sagawa, M.; Yamauchi, H. *J. Appl. Phys.* **1986**, *59*, 873.
(33) Salgueiro da Siva, M. A.; Moreira, J. M.; Mendes, J. A.; Amaral, V. S.; Sousa, J. B.; Palmer, S. B. *J. Phys.: Condens. Mater.* **1995**, *7*, 9853.
(34) Canfield, P. C.; Cho, B. K.; Dennis, K. W. *Phys. B* **1995**, *215*, 337.
(35) Garcia-Landa, B.; Tomey, E.; Fruchart, D.; Gignoux, D.; Skolozdra, R. *J. Magn. Magn. Mater.* **1996**, *157−158*, 21.
(36) Mendoza, W. A.; Shaheen, S. A. *J. Appl. Phys.* **1996**, *79*, 6327.
(37) Cao, G.; McCall, S.; Crow, J. E. *Phys. Rev. B* **1997**, *55*, R672.
(38) Kou, X. C.; Dahlgren, M.; Grössinger, R.; Wiesinger, G. *J. Appl. Phys.* **1997**, *81*, 4428.
(39) Herpin, A. *Théorie du Magnétisme*; Presses Universitaires de France: Paris, 1968.
(40) Shcherbakova, Ye. V.; Ivanova, G. V.; Bartashevich, M. I.; Khrabrov, V. I.; Belozerov, Ye. V. *J. Alloys Compd.* **1996**, 240, 101.
(41) Bozorth, R. M.; Chapin, D. M. *J. Appl. Phys.* **1942**, *13*, 320.

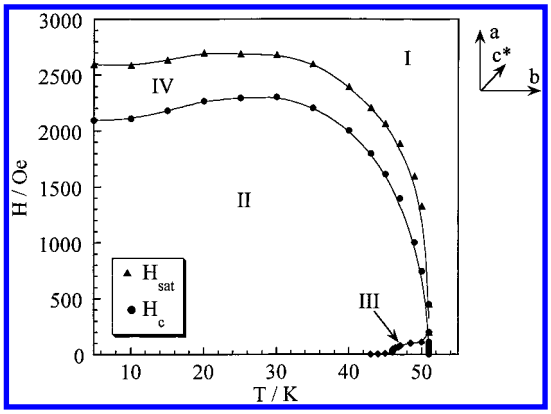

Figure 11. Magnetic phase diagram. The full lines are just eye-guides (see text).

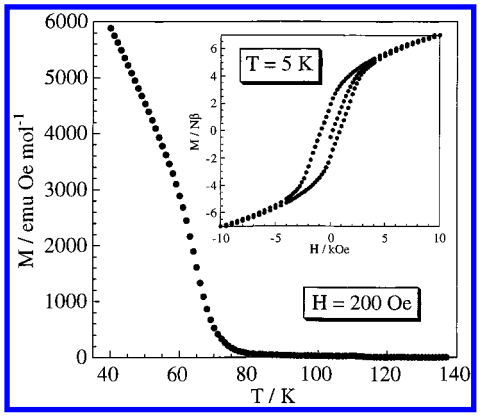

Figure 12. Temperature dependence of the magnetization for a dehydrated polycrystalline sample. In the insert is shown the field dependence of the magnetization at 5 K.

tion, M_s, at a given temperature may be determined by extrapolating the high-field magnetization down to $H = 0$. The temperature dependence of the spontaneous magnetization is shown in Figure 10 (bottom). It was obtained in applying the field along the *b* direction. As expected, the same temperature dependence of the spontaneous magnetization is obtained when applying the magnetic field along the *c** direction. On the other hand, a slightly different curve is obtained when applying the magnetic field along the *a* direction, which might result from the existence of the two ferromagnetic domains, II and III, as explained just below.

Magnetic Phase Diagram. Let us sum up the available information arising from the experimental magnetic data. The $Mo^{3+}-Mn^{2+}$ interaction through the cyano bridge is ferromagnetic. In zero or very weak external field two transitions are observed, one at 51 K and the other at 43 K. The former certainly corresponds to a transition between magnetically disordered and ordered states, and the latter to a transition between two magnetically ordered states. This latter transition is particularly evident when the weak field is applied along the *a* direction. As a matter of fact, two well-pronounced breaks are observed in the $M = f(T)$ curve along this direction (see Figure 8), and the magnetization below 43 K is higher than between 51 and 43 K. This transition at 43 K in zero field moves toward higher temperatures as the field increases and then merges with the transition at higher temperature as the field reaches 100 Oe. The *b* direction is the easy magnetization axis in low field. When a field along this direction is applied, a magnetic moment of 11 $N\beta$ is observed, which corresponds to the ferromagnetic alignment of the local spins. Finally, when a strong field along the *a* direction in the ferromagnetic phase is applied, a spin reorientation is observed for a critical value, H_c, of the field which first increases as *T* is lowered and then reaches ca. 2.2 kOe at 30 K. These data allow us to plot the temperature−magnetic field phase diagram represented in Figure 11. This diagram presents four domains. Domain I corresponds to high temperatures and/or high fields along *a*. It is the paramagnetic domain. When the field along *a* is high and the temperature low, the magnetic saturation is reached, but there is no phase transition between fully disordered paramagnetic state (high *T* and low *H*) and saturated paramagnetic state (low *T* and high *H*). Domain II corresponds to low temperatures and low field along *a*. It is a ferromagnetic domain in which resulting moment is aligned along the *b* direction. Domain III is limited to the 43−51 K temperature range and a field along *a* lower than 100 Oe. It corresponds to another ferromagnetically ordered state. Domain IV, finally, is limited by the $H_c = f(T)$ and $H_{sat} = f(T)$ curves and corresponds to a mixed domain in which the spins may rotate from the *b* to the *a* directions. It is difficult to specify the differences between the two magnetically ordered domains II and III. Assuming that the magnetic symmetry decreases as the temperature is lowered, one may assume that domain III is a strictly ferromagnetic domain in which the local spins are aligned along the *b* direction and that domain II is a canted ferromagnetic domain, with a component of the magnetic moment along the *a* direction. Alternatively, both domains II and III might correspond to canted ferromagnetic phases, the canting being more pronounced in domain II than in domain III. Only neutron diffraction data could allow us to determine unambiguously the nature of the two phases. We hope to be able to perform such a study in a near future. Interestingly, the canting is compatible with the crystal symmetry. The space group, $P2_1/c$, is centrosymmetric, but the Mn1 and Mn2 sites are crystallographically independent and, therefore, not symmetry related. It follows that there is no inversion center relating the spin carriers, and the antisymmetric interaction giving rise to spin canting may be operative.[42,43]

Magnetic Behavior after Dehydration. We already mentioned that the compound was unstable. This is true with respect not only to oxidation but to dehydration as well. Under vacuum, water molecules, probably the noncoordinated ones, are released, and the magnetic properties are strongly modified. Figure 12 shows the temperature dependence of the magnetization for a polycrystalline sample treated under vacuum at room temperature during 12 h and then sealed in a tube. The curve shows a break around 70 K, revealing a long-range magnetic ordering. The extremum of the derivative dM/dT is observed at $T_c = 65$ K. The field dependence of the magnetization is shown in the insert of Figure 12; it reveals a hysteresis loop with a coercive field of 0.85 kOe. Let us remind that for the hydrated material the coercive field is negligibly small. It is worth mentioning here that the stabilization of the ferromagnetic state upon dehydration of magnetic molecular materials has already been reported.[44−46]

Discussion

Origin of the Anisotropy. One of the remarkable features of the title compound is its strong magnetic anisotropy, which

(42) Dzialoshinsky, I. *J. Phys. Chem. Solids* **1958**, *4*, 241.
(43) Moriya, T. *Phys. Rev.* **1960**, *120*, 91.
(44) Nakatani, K.; Bergerat, P.; Codjovi, E.; Mathonière, C.; Pei, Y.; Kahn, O. *Inorg. Chem.* **1991**, *30*, 3977.
(45) Turner, S.; Kahn, O.; Rabardel, L. *J. Am. Chem. Soc.* **1996**, *118*, 6428.
(46) Larionova, J.; Chavan, S. A.; Yakhmi, J. V.; Gulbrandsen-Froystein, A.; Sletten, J.; Sourisseau, C.; Kahn, O. *Inorg. Chem.* **1997**, *36*, 6374.

raises the question of the origin of this anisotropy. The anisotropy of a magnetic single crystal is governed by both the shape of this single crystal and its chemical nature.[39] Let us first consider the shape factor. It is very difficult to determine accurately the shape anisotropy of a single crystal, except in a few cases of ideal structures, such as a sphere, an ellipsoid, or a cylinder (or a disk). However, we have shown that even when the raw data are approximately corrected of the demagnetizing effects, a pronounced anisotropy is retained. Therefore, the observed anisotropy is largely intrinsic in nature. The high-spin Mn^{2+} ion in octahedral surroundings is known to be very weakly anisotropic, with an azial zero-field splitting parameter within the $^6A_1$ ground state of the order of 10^{-2} cm^{-1} [47] and a quasi isotropic $\mathbf{g}_{Mn}$ tensor. The situation is a bit more complicated for low-spin Mo^{3+} in the $Mo(CN)_7$ environment. The ground state is $^2E''_1$, assuming an ideal pentagonal bipyramid (D_{5h}) geometry. The spin−orbit coupling together with the local distortion removes the 4-fold degeneracy to give rise to two Kramers doublets well separated in energy, and the $\mathbf{g}_{Mo}$ Zeeman tensor of the Kramers doublet of lowest energy may be very anisotropic. The principal values $g_x = g_y = 1.77$ and $g_z = 3.89$ have been reported for $NaK_3[Mo(CN)_7]\cdot 2H_2O$.[29] Furthermore, the $Mo^{3+}-Mn^{2+}$ interaction may have a significant anisotropic component, due to the spin−orbit coupling of Mo^{3+}. More precisely, such an anisotropic interaction would arise from the synergistic effect of the Mo^{3+} spin−orbit coupling and the interaction between the ground state of Mn^{2+} and the excited states of Mo^{3+}.[48,49] Finally, the structural anisotropy may also induce an anisotropy of the dipolar interactions, in particular between $S_{Mn} = {}^5/_2$ spins. Concerning the dipolar effects, an interesting remark can be made. We have seen in the section devoted to the description of the structure that the *b* direction corresponds to infinite bimetallic linkages of the type $(Mo-CN-Mn1-CN-)_n$. The Mo−CN−Mn interaction is ferromagnetic. In a ferromagnetic chain the dipolar interactions favor the alignment of the local spins along the chain direction and not perpendicularly to this direction.[50] This might explain why the *b* direction is the easy magnetization direction in low field.

One of the consequences of the magnetic anisotropy is the field-induced spin reorientation observed in the ferromagnetic domains. Spin reorientation results from the competition between magnetic interaction and magnetic anisotropy. In the present case, when the field overcomes a critical value, the *a* direction (i.e. the direction of the accordions) becomes as easy as (or even easier than) the *b* direction. So far, we have not succeeded to interpret this behavior from the structural data.

At the end of this paragraph, it is important to point out that despite the magnetic anisotropy the compound exhibits no coercivity, except for the dehydrated form. The single crystal of $Mn_2(H_2O)_5Mo(CN)_7\cdot 4H_2O$ is multidomain, and the domain walls move freely with the field. The coercivity is due to both chemical and structural factors.[51] As far as the chemical factors are concerned, the key role is played by the local anisotropy of the spin carriers. In the present case, 10 out of 11 active electrons come from the isotropic Mn^{2+} ions. The pertinent structural factors are the grain shape and size along with the structural defects on which the domain walls can be pinned. These structural defects probably explain why the partially dehydrated compound exhibits a magnetic hysteresis, with a coercive field of 0.85 kOe at 5 K. As a matter of fact, the crystal structure after release of noncoordinated water molecules is most likely strongly disordered.

Ferromagnetic Nature of the $Mo^{3+}-Mn^{2+}$ Interaction. The $Mo^{3+}-Mn^{2+}$ interaction through the cyano bridge was found to be ferromagnetic. This situation was not anticipated, and we discuss briefly the possible mechanisms which could lead to a parallel alignment of the local spins.

Active Electron Approximation. The one-electron energy diagrams for low-spin Mo^{3+} in pentagonal bipyramid symmetry and high-spin Mn^{2+} in octahedral symmetry are recalled. At

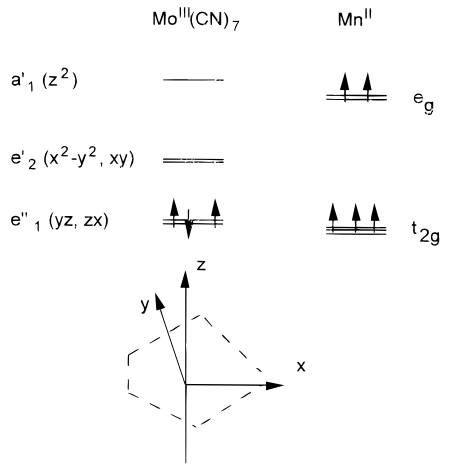

the active electron approximation the interaction parameter J occurring in the spin Hamiltonian $-J\mathbf{S}_{Mo}\cdot\mathbf{S}_{Mn}$ may be written as[49]

$$J = (1/5)\sum_{i=1-5} J_i \qquad (3)$$

where J_i refers to the interaction between the singly occupied orbital of Mo^{3+} and one of the five singly occupied orbitals describing the unpaired electrons of Mn^{2+}. These singly occupied orbitals are defined as the magnetic orbitals of the system. In the D_{5h} symmetry the unpaired electron of Mo^{3+} occupies a e''_1 orbital, with a π character with respect to both equatorial and axial Mo−C−N directions. The unpaired electrons of Mn^{2+} occupy the three t_{2g} and two e_g orbitals; one of them gives a nonzero overlap integral with the magnetic orbital of Mo^{3+}; the interaction between these two magnetic orbitals gives an antiferromagnetic (AF) contribution, e.g. J_1. The other four are orthogonal to the magnetic orbital of Mo^{3+}, which gives four ferromagnetic (F) contributions, e.g. J_2-J_5. In the Prussian blue-like phases the AF contributions dominate the F contributions, even when they are less numerous.[14,49] For instance, $Mn_3[Fe(CN)_6]_2\cdot 15H_2O$ is a ferrimagnet and not a ferromagnet, with $T_c = 9$ K.[12] The overall interaction between low-spin Fe^{3+} ion with one unpaired electron in the t_{2g} orbitals and high-spin Mn^{2+} ion with three unpaired electrons in the t_{2g} and two in the e_g orbitals is AF. In the present case the sum of the F contributions, J_2-J_5, might overcome the single AF contribution, J_1. Let us mention that the arguments above lie on ideal D_{5h} and O_h local symmetries along with linear Mo−C−N−Mn linkages. Any lowering of symmetry removes the strict orthogonality of magnetic orbitals and, therefore, is expected to disfavor the F interaction.

(47) Abragam, A.; Bleaney, B. *Electron Paramagnetic Resonance of Transition Ions*; Dover Publications: New York, 1970.

(48) Bencini, A.; Gatteschi, D. *EPR of Exchange Coupled Systems*, Springer-Verlag: Berlin, 1990.

(49) Kahn, O. *Molecular Magnetism*; VCH: New York, 1993.

(50) Caneschi, A.; Gatteschi, D.; Renard, J. P.; Rey, P.; Sessoli, R. *Inorg. Chem.* **1989**, *28*, 3314.

(51) Vaz, M. G. F.; Pinheiro, L. M.; Stumpf, H. O.; Alcantara, A. F. C.; Golhen, S.; Ouahab, L.; Cador, O.; Mathonière, C.; Kahn, O. *Chem. Eur. J.*, submitted for publication.

Role of Charge-Transfer Configurations. Let us briefly recall that the ground configuration for each $Mo^{3+}-Mn^{2+}$ pair, $e''_1-t_{2g}^3e_g^2$, may mix with excited charge transfer configurations, provided that these latter are not too high in energy. When the excited configuration arises from an electron transfer from a singly occupied orbital on a site to a singly occupied orbital on the other site, the mixing favors the AF interaction.[52] On the other hand, when the excited configuration arises from an electron transfer from a singly occupied orbital on a site to an empty orbital on the other site, or alternatively from a doubly occupied orbital on a site to a singly occupied orbital on the other site, then the mixing favors the F interaction.[53] In the present case, both types of excited states exist. Among them, those involving a σ electron transfer from a e_g singly occupied orbital of Mn^{2+} to one of the $a'_1 + e'_2$ empty orbitals of Mo^{3+} might give strong F contributions.

Spin Polarization of the $Mo(CN)_7$ Core. At the self-consistent field (SCF) level the e'_2 ($x^2 - y^2$, xy) and a'_1 (z^2) orbitals of the pentagonal bipyramid fragment $Mo^{III}(CN)_7$ with a predominant 4d character are empty. It follows that, at this approximation level, there is no spin density along both equatorial and axial Mo−C−N directions. It is now well established that such a view is oversimplified. The $^2E''_1$ SCF ground state may couple with SCF excited states of the same symmetry in which electrons have been promoted from the doubly occupied and bonding e'_2 and a'_1 orbitals with a predominant cyano character to the empty and antibonding e'_2 and a'_1 orbitals with a predominant metal character. This configuration interaction gives rise to a negative spin density in the σ orbitals of the cyano ligands, along the Mo−C−N directions. This spin polarization effect has been experimentally observed in the hexacyanometalates involving 3d ions, such as $[Cr(CN)_6]^{3-}$ and $[Fe(CN)_6]^{3-}$, from polarized neutron diffraction experiments.[54,55]

The important point is that the stronger (i.e. the more covalent) the M−(CN) bond is, the more pronounced the spin polarization. Owing to the diffuseness of the 4d orbitals as compared to the 3d orbitals, the Mo^{III}−(CN) bond is significantly stronger than the Cr^{III}−(CN) or Fe^{III}−(CN) bond. It follows that the negative spin density in the $Mo(CN)_7$ fragment might be particularly important. If it was so, the interaction between this negative spin density with a σ character and the σ singly occupied orbitals of Mn^{2+} might favor the parallel alignment of the S_{Mo} and S_{Mn} spins. This mechanism, based on a spin polarization effect specific to the 4d metal ions, seems to us to be particularly relevant; we are presently exploring this mechanism further through DFT calculations.

Conclusion

The studies concerning the Prussian blue-like phases, in particular those performed by Girolami and Verdaguer in the past few years, have provided very important insights on the magnetism of polymetallic compounds obtained from molecular precursors. Perhaps, the most remarkable result concerns the rational design of high-temperature magnets, using the theoretical models developed in molecular magnetism. In this respect, the high symmetry of the structure is a favorable condition to monitor the magnetic properties in a rational way. Indeed, the nature of the interaction between spin carriers is governed by symmetry rules involving the singly occupied orbitals.[49] When the symmetry is lowered, these rules become less heuristic. In particular, the situation of strict orthogonality of the magnetic orbitals leading to F interactions vanishes.

The work described in this paper does not lie in the same line of research. What we attempted to do is to lower the symmetry in order to observe anisotropic effects and to see to what extent this lowering of symmetry would lead to new phenomena. Powder measurements may provide most of the pertinent information when the compounds crystallize in cubic space groups. On the other hand, single-crystal measurements become essential when working with low-symmetry systems. Therefore, it was crucial for us to be capable to grow single crystals. The reaction of $[Mo(CN)_7]^{4-}$ with Mn^{2+} ions not only gives well-shaped single crystals of the α phase investigated in this paper but also of a β phase which a subsequent paper will be devoted to. $[Mo(CN)_7]^{4-}$ was obviously a good candidate to design a low-symmetry extended network. Indeed, the hepta-coordination is not compatible with a cubic symmetry.

$Mn_2(H_2O)_5Mo(CN)_7 \cdot 4H_2O$ not only is a ferromagnet in which the local spins tend to align along the *b* direction but also exhibits two magnetically ordered states; only polarized neutron diffraction studies will allow us to specify the differences between these two phases. Furthermore, when the external field is applied along the *a* direction, i.e., the direction of the accordions made of edge sharing lozenge motifs, a field-induced spin reorientation is observed. Both *a* and *b* become easy magnetization axes.

Another interesting result concerns the pronounced increase of the critical temperature as the compound is partially dehydrated together with the occurrence of a hysteresis loop. The structure of the partially dehydrated material is not known, so that it is not possible to explain this evolution between initial and partially dehydrated compounds. However, one can anticipate that the $Mo^{3+}-C-N-Mn^{2+}$ interaction parameter is not substantially modified through the dehydration process. At this stage, it is worthwhile to estimate the magnitude of the interaction parameter, *J*, between Mo^{3+} and Mn^{2+} ions, using the mean field approximation. Adapting Neel's approach[56] to the case where there are three magnetic sites, each of them with a different number of nearest neighbors, results in

$$T_c = (z_{Mo}z_{Mn1}z_{Mn2}C_{Mo}C_{Mn1}C_{Mn2})^{1/3}J/(Ng^2\beta^2)^{1/3} \qquad (4)$$

where $z_{Mo} = 7$, $z_{Mn1} = 4$, and $z_{Mn2} = 3$ are the number of nearest neighbors and C_{Mo}, C_{Mn1}, and C_{Mn2} are the Curie constants of the Mo, Mn1, and Mn2 sites, respectively. Equation 4 leads to $J = 6.3\ cm^{-1}$.

In this paper, we did not present all the physical data already available for $Mn_2(H_2O)_5Mo(CN)_7 \cdot 4H_2O$. Rather, we selected some of the most pertinent data and showed how they allow us to establish the peculiar magnetic phase diagram of the material. Other physical properties will be reported soon in more specialized journals.

Supporting Information Available: Listings of crystal and structure refinement data, atomic coordinates, bond lengths and angles, and anisotropic displacement parameters (7 pages, print/PDF). See any current masthead page for ordering information and Web access instructions.

JA9739953

(52) Anderson, P. W. In *Magnetism*; Rado, G. T., Suhl, H., Eds.; Academic Press: New York, 1963; Vol. 1, p 25.

(53) Goodenough, J. B. *Phys. Rev.* **1955**, 100, 564; *J. Phys. Chem. Solids* **1958**, 6, 287.

(54) Figgis, B. N.; Forsyth, J. B.; Reynolds, P. A. *Inorg. Chem.* **1987**, *26*, 101.

(55) Figgis, B. N.; Kucharski, E. S.; Vrtis, M. *J. Am. Chem. Soc.* **1993**, *115*, 5, 176.

(56) Neel, L. *Ann. Phys.* **1948**, *3*, 137.